Wear 332-333 (2015) 1151–1157

Contents lists available at ScienceDirect

Wear

journal homepage: www.elsevier.com/locate/wear

Oxidation wear monitoring based on the color extraction of on-line wear debris

Yeping Peng [a,b], Tonghai Wu [a,*], Shuo Wang [a], Zhongxiao Peng [b]

[a] Key Laboratory of Modern Design and Rotor Bearing System of Ministry, Xi'an Jiaotong University, Xi'an 710049, Shaanxi, People's Republic of China
[b] School of Mechanical and Manufacturing Engineering, The University of New South Wales, Sydney, NSW 2052, Australia

ARTICLE INFO

Article history:
Received 14 September 2014
Received in revised form
15 December 2014
Accepted 29 December 2014
Available online 5 January 2015

Keywords:
Oxidation wear
On-line monitoring
Color extraction
Wear debris

ABSTRACT

Oxidation associated wear usually involves high temperature and often accelerates lubrication degradation and failure processes. The color of oxide wear debris highly corresponds with the severities of oxidation wear. Therefore, on-line detection of oxide wear debris has the advantage of revealing the wear condition in a timely manner. This paper presents a color extraction method of wear debris for on-line oxidation monitoring. Images of moving wear particles in lubricant were captured via an on-line imaging system. Image preprocessing methods were adopted to separate wear particles from the background and to improve the image quality through a motion-blurred restoration process before the colors of the wear debris were extracted. By doing this, two typical types of oxide wear debris, red Fe_2O_3 and black Fe_3O_4, were identified. Furthermore, a statistical clustering model was established for automatic determination of the two typical types of oxide wear particles. Finally, the effectiveness of the proposed method was verified by performing real-time oxidation wear monitoring of experimental data. The proposed method provides a feasible approach to detect early oxidation wear and monitor its progress in a running machine.

1. Introduction

Metallic oxidation, often caused by high temperature at metal-to-metal contacts due to overload and/or lack of lubrication, is one of the main causes of tribological failures. High flash temperature generated in the wear process will not only tender the tribo materials but also deteriorate the lubricant in use. Therefore, early detection of oxidation wear is of significance for preventive maintenance of mechanical systems [1,2].

Wear debris is the direct by-product generated in a wear process and contains valuable information about machine conditions. Thus the features of wear debris are characterized for machine condition monitoring and fault diagnosis. Among these features, the colors of wear debris are used as critical information for oxide wear debris identification. For instance, the predominant oxide products of most tribo-systems made of steel (Fe–C alloy) are Fe_2O_3 and Fe_3O_4, which can be identified by examining their special colors. In addition, the oxide films of low alloy steel, from inside to outside, are FeO (FeO cannot be produced under 600 °C), Fe_3O_4 and Fe_2O_3 layer [3]. If the oxidation film breaks up to form wear debris, it means that severe wear with a high wear rate occurs and the types of oxide wear particles can reveal the wear degree. At present, color-based classification of oxide wear debris has been studied extensively and accepted as a theoretical base for oxidation wear analysis [4,5].

Color extraction of wear debris is an essential step for oxidation wear monitoring using off-line analysis techniques. Myshkin [4] used optical microscopy to acquire wear debris images and extract their colors. By using a multi-scale classification criterion, wear particles were classified into red oxide (Fe_2O_3) and black oxide (Fe_3O_4) based on their colors. Compared with off-line approaches such as Myshkin's work, on-line monitoring technology has the advantage of capturing real-time machine data [6,7]. Color images of wear debris can also be captured using on-line ferrograph technology to identify wear sources. Identification of some typical metal particles, including copper, iron and aluminum debris was achieved through extracting their colors from on-line images [8]. However, this method is effective only when wear debris images are clear. Unfortunately, wear debris images sampled with an online sensor are often fuzzy because of a number of reasons, e.g. the movements of the particles and lubricant. Also, reported on-line monitoring systems applied the ferrograph approach to capture iron particles [9]. Consequently, the particles are often in a chain pattern and overlapping, which make it difficult to separate wear particles. Color recognition of moving wear debris thus remains a bottleneck for on-line wear monitoring.

Video-based image processing technology provides a new approach for dynamic characteristics extraction, and has been

* Corresponding author. Tel.: +86 29 82669161.
E-mail address: wt-h@163.com (T. Wu).

http://dx.doi.org/10.1016/j.wear.2014.12.047
0043-1648/

successfully applied in medical diagnosis [10], robot vision [11] and intelligence transportation [12]. Specifically, video acquisition can avoid the agglomeration of motion particles to achieve accurate characteristics extraction of multiple wear particles. Although the motion of wear debris introduces image blurring, color information can be obtained using color image enhancement methods [13,14].

Aiming at on-line oxidation wear monitoring, this work investigated the color extraction of wear debris from on-line sampled images. An image capturing system was constructed to acquire the color images of moving wear particles. To extract the colors of wear debris effectively, the methods of improving on-line images quality were studied, the color information was extracted, and wear particles were classified based on their colors for on-line oxidation wear monitoring. The practicability of the proposed method was evaluated experimentally using a four-ball wear tester.

2. Dynamic wear debris image acquisition system

An experimental system for oxidation wear testing and monitoring was designed and is illustrated in Fig. 1. A typical four-ball wear tester was adopted as a testing machine that the on-line monitoring equipment was set up on. Particles produced by the friction pair flew into the oil tank and then were directed to the designed oil flow path by a digital pump. Videos of dynamic wear debris were captured using a video sensor with light-emitting diodes (LED). A single chip microcomputer was utilized to drive the digital pump and the LED. To avoid the circulation of analyzed particles in the oil system, an oil bottle was set up in the return pipe. The clean oil in the upper portion of the oil bottle was drained by another digital pump into the oil tank. The return oil with wear debris was sent to the bottom of the oil bottle so the particles could be deposited.

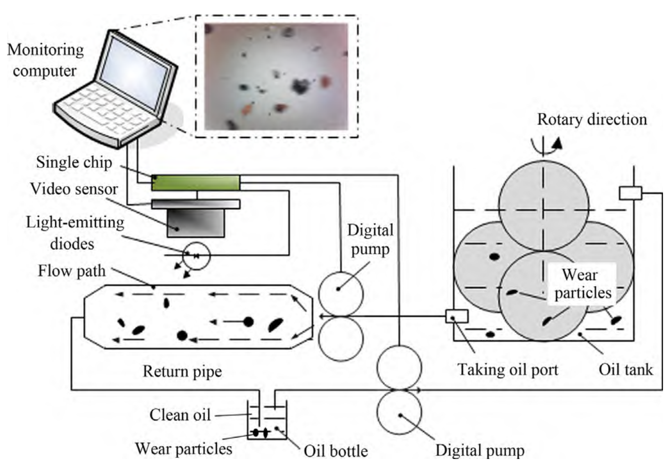

Fig. 1. Schematic illustration of the on-line monitoring equipment installed on a four-ball rig.

The videos of dynamic particles were processed to extract particle images. A typical wear debris image extracted from the video stream is shown in Fig. 2(a). As can be seen, wear particles in different colors were captured. By comparing with the analytical ferrograph image in Fig. 2(b), two drawbacks of the on-line image are revealed.

1) The background varies with light conditions and oil transparency, resulting in a low contrast between the particles and background.
2) The resolution of the on-line image is less than that of an off-line ferrograph image, which is caused by the movement of the particles and lubricant involvement.

These issues make it difficult to extract the color information of the wear debris. In order to effectively extract the information, the background of the image needs to be segmented and the image quality needs to be improved. Details of the wear debris image segmentation and enhancement methods will be presented in the next section.

3. Color extraction of dynamic wear debris

Images of moving particles captured by the video acquisition system contain their color features for particle identification. However, it is difficult to extract color information from the dynamic image because of the two issues described in Section 2. Thus image segmentation and color enhancement are necessary before acquiring useful color information.

3.1. Color segmentation of wear debris image

As depicted in Fig. 2, a particle image can be divided into two parts: wear debris and background. For image segmentation, a background subtraction method [15] was employed to separate the wear debris. A series of images were extracted from a video clip to reconstruct a real-time background of the images. Fig. 3 gives nine frames selected from the images sampled in 12 s. The

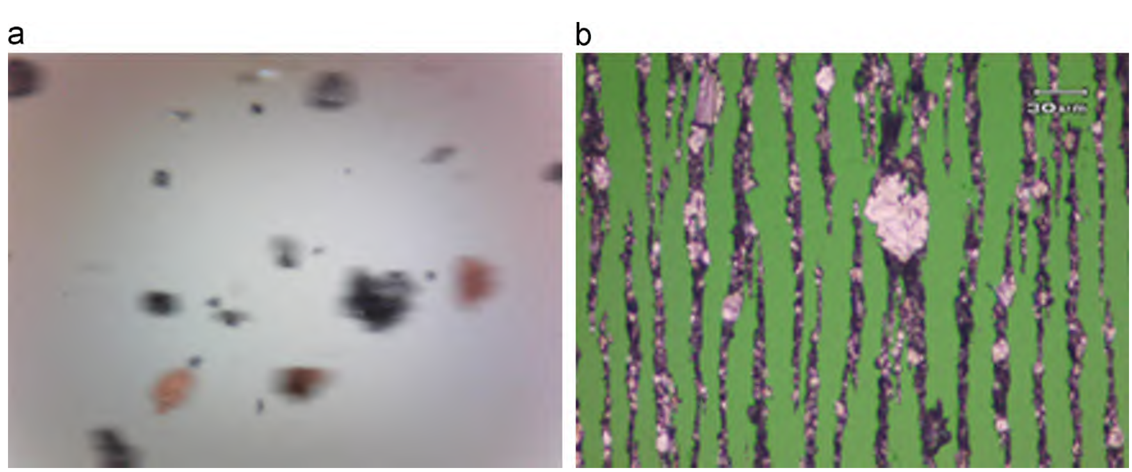

Fig. 2. Typical images carried by on-line monitoring equipment and analytical ferrography: (a) on-line acquisition image and (b) analytical ferrograph image.

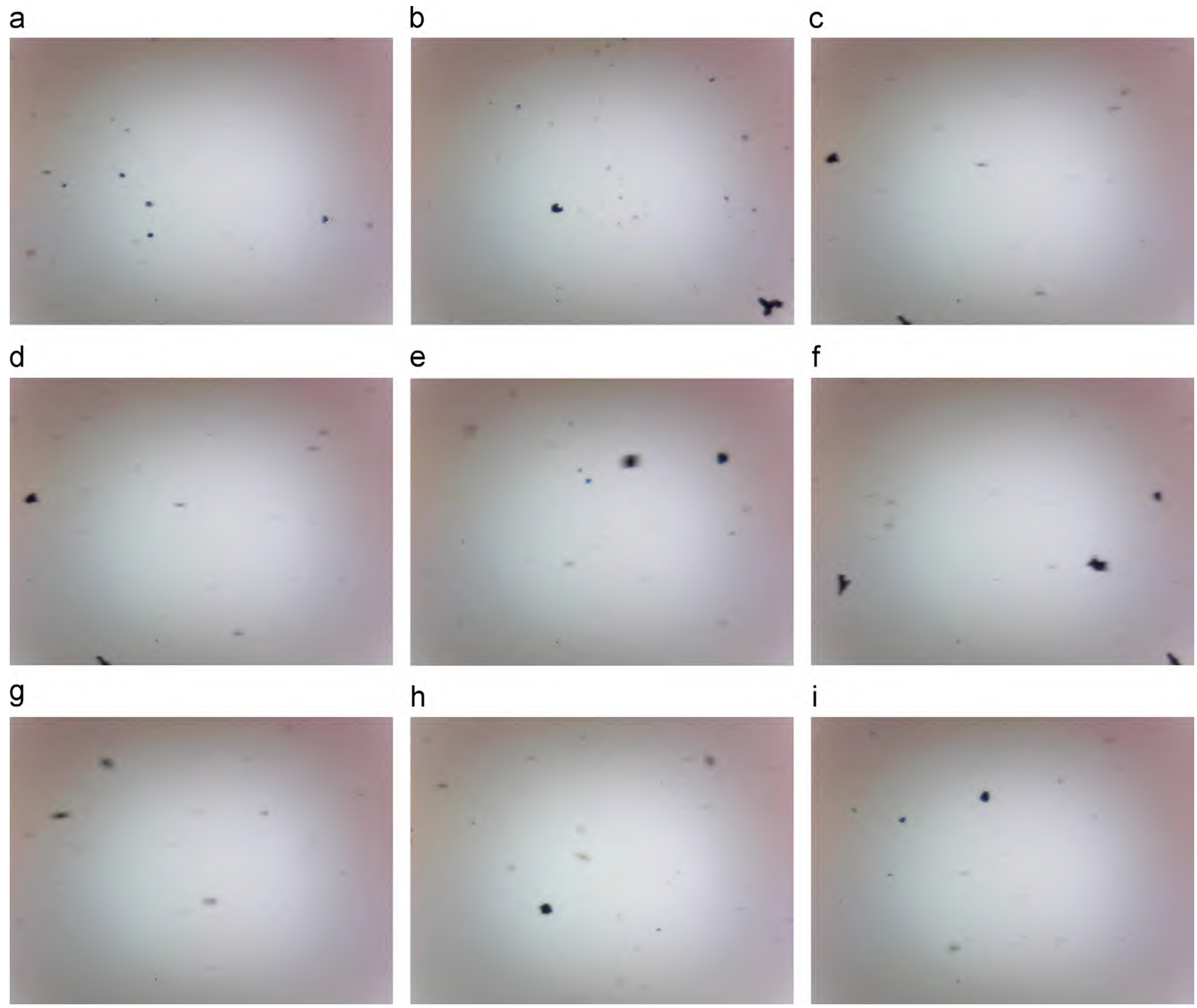

Fig. 3. Some image frames extracted from wear debris video: (a) 50 frame, (b) 100 frame, (c) 150 frame, (d) 200 frame, (e) 250 frame, (f) 300 frame, (g) 350 frame, (h) 400 frame and (i) 450 frame.

Gaussian background modeling method [16] was adopted to reconstruct the background using those image frames (600 frames) after gray processing. An example of a reconstructed background image is shown in Fig. 4.

Fig. 4 is a background image after the wear debris and artificial colors shown in Fig. 3 were removed. The difference between Fig. 2(a) and Fig. 4 was computed using the background subtraction method mentioned above to acquire a color image of wear debris, and the resultant image is shown in Fig. 5. As can be seen, the wear debris was well segmented from the background. However, the low resolution issue still needs to be resolved.

3.2. Enhancement of on-line wear debris images

A number of filters including Wiener filter [17] and median filter [18] were proposed for color image enhancement. As stated before, the dynamic particle images appear blurring mainly caused by the motion of particles and random noise. Considering that random noise needs to be removed and that the Wiener filtering can minimize the mean square error between restored and sharp images, it was adopted as the filtering method in this work.

Fig. 6 shows the degradation model of a blurred image. As illustrated in the degradation model, a degraded image represented using $g(x, y)$ results from the convolution between a sharp image $f(x, y)$ and a degradation function $h(x, y)$ and is also affected by noise $n(x, y)$.

Fig. 4. The reconstructed background image based on the wear debris images shown in Fig. 3.

The relationship between blurred and sharp images can be described as

$$g(x,y) = f(x,y) * h(x,y) + n(x,y) \tag{1}$$

where $*$ denotes the linear convolution.

Image restoration is the inverse operation of image degradation. The Wiener filtering method has superior performance in denoising [19], but the degradation function $h(x, y)$ still needs to be performed to check the image restoration outcome. The relative motion of particles to the video sensor is the main reason for image blurring. The $h(x, y)$ for motion blur can be expressed by [17]

$$h(x,y) = \begin{cases} 1/L, & \sqrt{x^2+y^2} \le L/2, \quad y/x = \tan\theta \\ 0, & \text{else} \end{cases} \tag{2}$$

where L is the length of blur; θ is the angle of blur.

Consequently, the parameters estimation of the blur angle θ and length L is of significance for motion-blurred image restoration. Generally, the wear debris motion can be simplified as uniform linear motion at a constant velocity v and a blur direction θ when the exposure time is short. During the exposure time interval [0, T], the blur length can be calculated using $L = vT$. Fig. 2(a) shows sampled in the conditions that the average speed of wear debris was 2.4 mm/s and the video sampling rate was 50 frames per second (fps) with a resolution of 640 × 480 pixels. Considering the scale factor of 1.5 μm per pixel, the length of blur L was calculated to be 32 pixels.

In addition, Fourier spectrum has been widely used to obtain the motion-blurred angle of an image [20]. Parallel stripes will be found in the frequency spectrum image if there is motion blurred direction. With 90° clockwise rotation of the angle between the parallel stripes and horizontal axis, the blur angle θ can be confirmed. Based on this theory, the Fourier transform result of the dynamic wear debris image (Fig. 7(a)) is shown in Fig. 7(b). As can be seen, nearly no parallel stripes can be found in the middle of the spectrum image. This is because the direction of the particle movement is parallel to the video sensor as shown in Fig. 1. Thus the motion direction of the wear debris can be regarded as horizontal direction, namely $\theta = 0$, in the short exposure interval.

The motion-blurred image of dynamic wear debris was restored by utilizing the Wiener filtering method with the blur angle $\theta = 0$

Fig. 5. Wear debris image after excluding the background (Fig. 4) from the initial on-line image shown in Fig. 2(a).

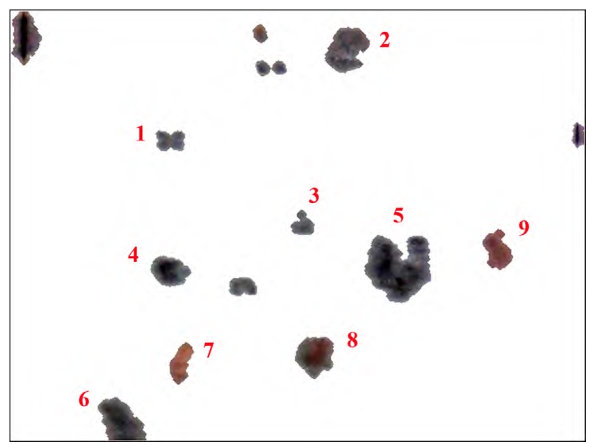

Fig. 8. The segmentation and restoration image of Fig. 7(a).

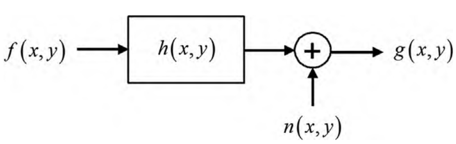

Fig. 6. The degradation model of motion-blurred.

Table 1
Results of H and I extraction of the wear debris in Fig. 8.

Debris number	1	2	3	4	5	6	7	8	9
H /degree	0.66	0.74	0.50	0.90	0.73	0.60	**0.18**	**0.02**	**0.13**
I /dimensionless	0.38	0.28	0.30	**0.06**	**0.13**	**0.19**	0.28	0.36	0.14
Particles color	other	other	other	black	black	black	red	red	red

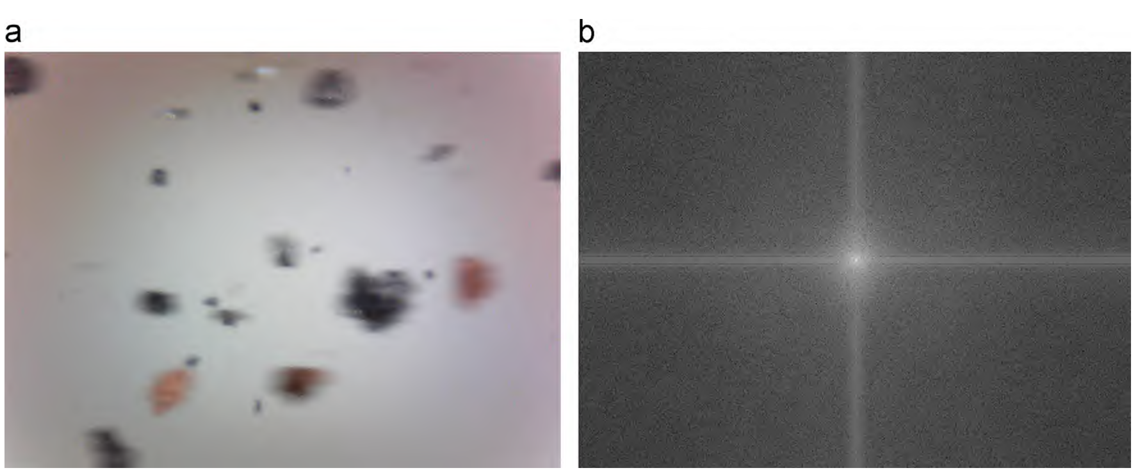

Fig. 7. Fourier transform result of a wear debris image: (a) dynamic wear debris image and (b) its Fourier spectrum image.

and the blur length $L=32$ pixels, and the result is shown in Fig. 8. Clearer particles are displayed in the restoration image than those in Fig. 5. The processed image is appropriate for wear debris color extraction. It is worth noting that the image separation and restoration process does not alter the color information of the particles.

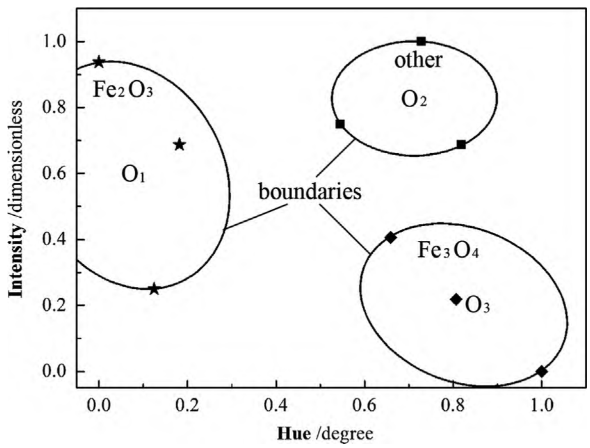

Fig. 9. The training result of the identification model with the data in Table 1.

3.3. Color extraction of wear debris

A color image can be expressed by two models including red, green and blue (RGB) color model and hue-saturation-intensity (HSI) model. R, G and B denote the pixels in the corresponding color channels of a color image, which can be directly extracted using computer software. The HSI model can be converted from the RGB model.

According to the previous work [8], wear debris classification was achieved based on the combined hue and intensity components of HSI color space. Hence, this study adopted the indexes of hue and intensity to distinguish oxide wear debris. The hue and intensity components can be transformed from R, G and B components as follows [8]:

$$H=\begin{cases}\theta & ,\text{if } B\le G\\ 360-\theta & ,\text{if } B>G\end{cases} \tag{3}$$

$$I=\frac{1}{3}(R+G+B) \tag{4}$$

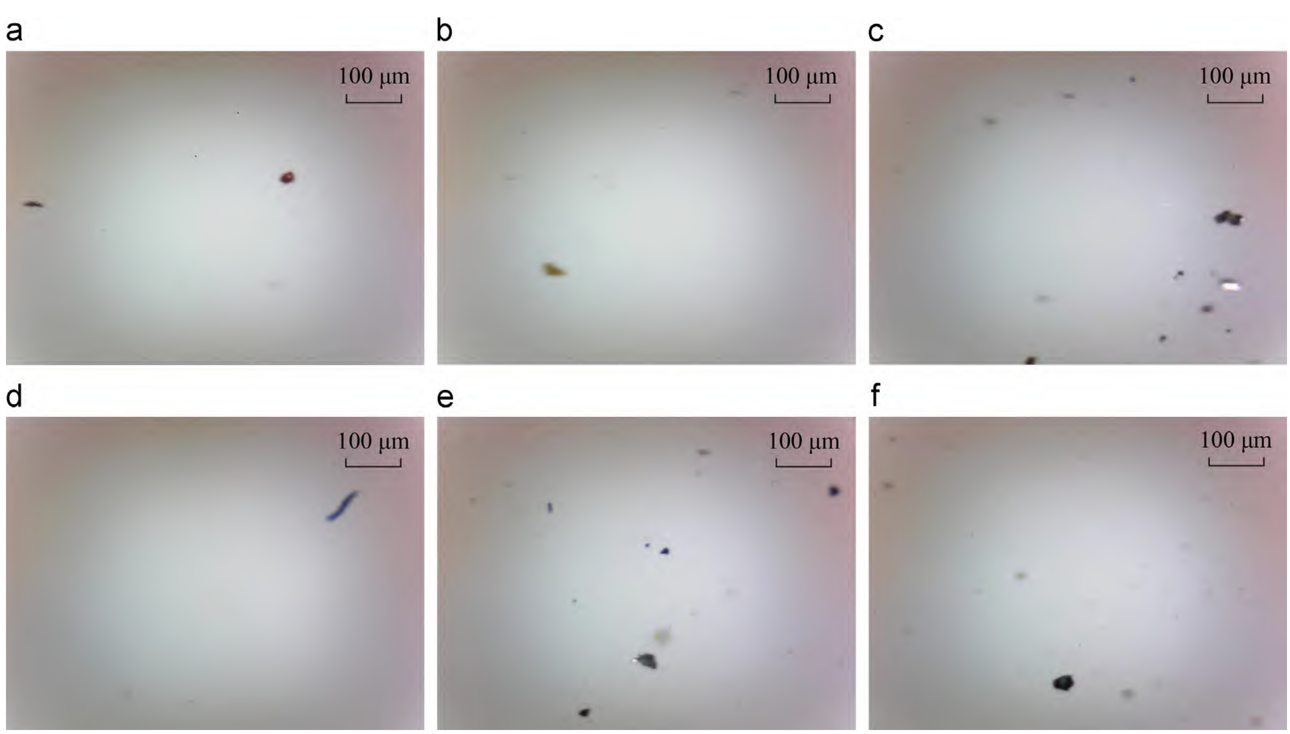

Fig. 10. Six typical wear debris images captured in the four-ball test monitoring: (a), (b), (c), (d), (e) and (f).

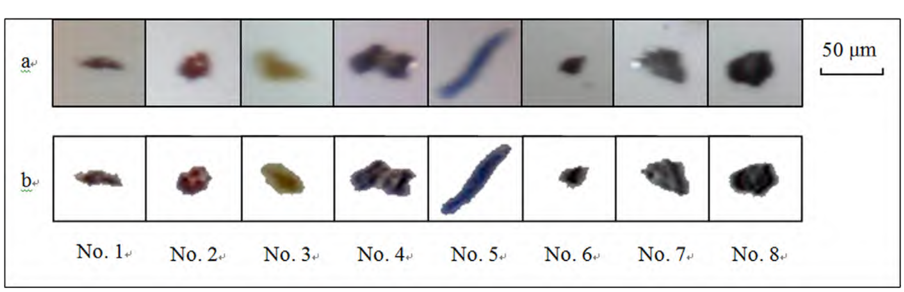

Fig. 11. Image enhancement by applying the segmentation and restoration methods to the particles: (a) the extracted wear debris from Fig. 10 and (b) the improved particle images of (a).

where,

$$\theta = \arccos\left\{\frac{1/2[(R-G)+(R-B)]}{\left[(R-G)^2+(R-B)(G-B)\right]^{1/2}}\right\} \tag{5}$$

where H, S and I are the three components of the HSI model. The value ranges of R, G and B components are normalized between 0 and 1 here.

The extraction results of the HSI components of the wear debris in Fig. 8 are shown in Table 1. It can be seen from the table that, based on the indexes of the hue and intensity, the marked particles were categorized into three groups named as black, red or other. Particles No. 7–9 were firstly identified to be red because they had smaller hue values than the others. Second, the black particles of No. 4–6 were separated because their intensities were less than those of particles No. 1–3.

4. Multi-class classification of oxide particles based on support vector data description

Two typical types of oxidation wear products including red oxide (Fe_2O_3) and black oxide (Fe_3O_4) are concerned in this study. For on-line monitoring, a dynamic clustering model of oxide wear debris identification was established with a multi-class classifier based on support vector data description (Multi-SVDD) [21,22].

4.1. Oxide wear debris identification model based on Multi-SVDD

In this study, all particles were categorized into one of the three groups, that is, Fe_2O_3, Fe_3O_4 and other, based on their indexes of H and I. A large amount of the data (H, I) of each group were clustered by SVDD to find the boundaries of the three sets. A newly captured particle was classified automatically through calculating the shortest distance between the particle and the boundaries. To train the classification model, the samples in Table 1 were used as training data. The hue and intensity values in Table 1 were normalized using

$$H'(i) = \frac{H(i) - \min(H)}{\max(H) - \min(H)}, \quad i = 1,\ 2, \ldots,\ n \tag{6}$$

$$I'(i) = \frac{I(i) - \min(I)}{\max(I) - \min(I)}, \quad i = 1,\ 2, \ldots, n \tag{7}$$

where, $H'(i)$ and $I'(i)$ are the normalized values of hue and intensity; $H(i)$ and $I(i)$ are the original values of hue and intensity; max(.) and min(.) are the maximum and minimum of all values, respectively; n is the number of all particles.

Fig. 9 shows the training outcome using the data of the particles listed in Table 1. As can be seen, the training model was correctly established using the Multi-SVDD approach for oxide particle classification. Although the identification model shows a satisfied result, more particle samples in other colors need to be used to update the model so it can identify a wider range of oxide wear debris. By training the model with more particles, the identification results will be more reliable.

4.2. Application of oxide wear debris identification

For on-line oxidation wear monitoring, an application of the identification model was carried out on the four-ball on-line monitoring test rig shown in Fig. 1. A 4 h wear test was conducted at a speed of 1000 r/min and a load of 1500 N. The digital pump drained the lubricant with a flow rate of 1 mL/min. Videos of dynamic wear debris were sampled at a sampling rate of 50 fps, and the images were presented in a true color format with a resolution of 640 × 480 pixels.

Fig. 10 shows six typical images of wear debris generated in the test. It can be seen that the particles had different colors and the background also varied in color. The extracted particles from the images in Fig. 10 are displayed in Fig. 11(a). As can be seen, the original images are fuzzy due to the particle motion. By applying the color image segmentation and enhancement techniques described in Sections 3.1 and 3.2, the quality of the final wear debris images shown in Fig. 11(b) was improved significantly.

The hue and intensity values of the wear debris were extracted for particle identification. The identification results using the trained model are given in Table 2. Fe_2O_3, Fe_3O_4 and other particles were marked to be “1”, “2” and “3” respectively. The results reveal that oxide wear debris was produced during the test, which indicates the occurrence of oxidation wear.

Table 2
The values of H and I of the wear debris in Fig. 11.

Particles	No. 1	No. 2	No. 3	No. 4	No. 5	No. 6	No. 7	No. 8
H /degree	0.81	0.21	0.11	0.81	0.65	0.68	0.41	0.64
I /dimensionless	0.30	0.32	0.29	0.25	0.23	0.05	0.28	0.11
Particle type	3	1	1	3	2	2	3	2

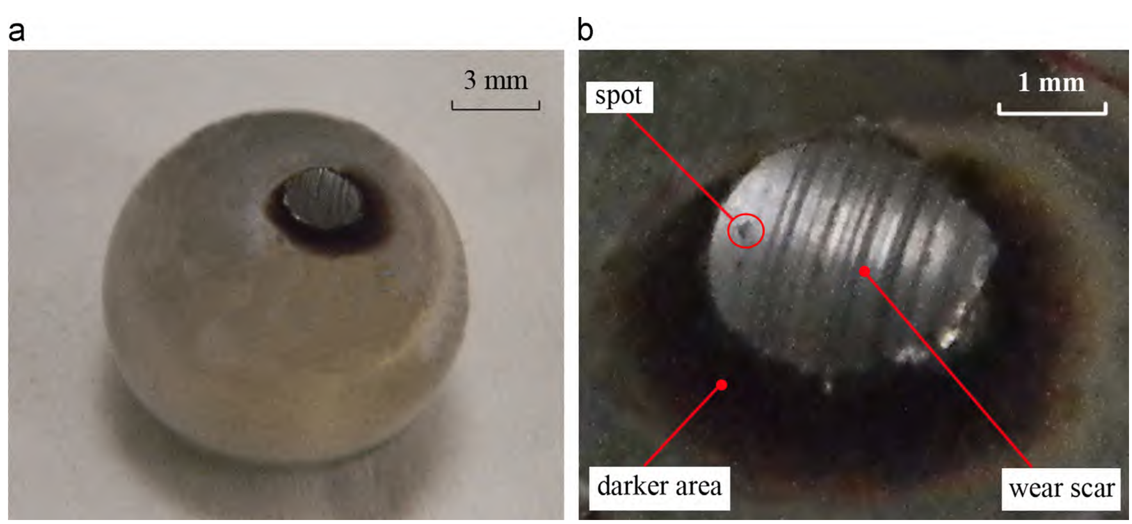

Fig. 12. Images of the worn steel ball: (a) image of the ball and (b) enlarged image of the worn surface.

To further verify the identification results, the tested steel balls were checked and the wear condition is shown in Fig. 12. As can be seen from Fig. 12(b), the radius of the wear scar is nearly 1.25 mm, and the color around the wear scar is darker than other areas. This is because a large amount of heat was generated at the metal–metal contacts during the sliding motion. Metallic oxidation occurred under high temperature turning the material into a black color. At the same time, the oxidation surface of the friction pair was worn away during wear. Thereafter, oxidation continued and local oxidation spot appeared.

5. Conclusions

Aiming at monitoring oxidation wear in a running machine, an on-line oxide wear debris identification method was established by focusing on the color feature extraction of dynamic wear particles. The color extraction from a blurred image of moving wear debris was studied to characterize different types of oxide wear debris. The following conclusions can be drawn.

1) A video-based imaging system was adopted to acquire real-time color images of moving particles. To solve the blurring problem associated with these on-line images, the image segmentation and restoration methods were proposed to improve the image quality.
2) The hue and intensity components of the HSI model were utilized for oxide wear debris classification. By using a Multi-SVDD classifier, two typical types of wear particles, red Fe_2O_3 and black Fe_3O_4, were identified.
3) Experiment results proved that real-time oxidation wear monitoring can be realized using the method of color extraction developed in this work. This development is potentially useful for industry applications.

Acknowledgments

The financial support of the present research was provided by the National Science Foundation of China (Grant nos. 50905135, 51275381) and the Science and Technology Planning Project of Shaanxi Province, China (Grant no. 2012GY2-37). Special thanks to the financial support from the China Scholarship Council (Grant no. 201406280050) during the term of this project.

References

[1] C.Q. Yuan, Z. Peng, X.C. Zhou, X.P. Yan, Effects of temperature on sliding wear process under contaminated lubricant test conditions, Wear 257 (2004) 812–822.
[2] X.H. Cui, S.Q. Wang, F. Wang, K.M. Chen, Research on oxidation wear mechanism of the cast steels, Wear 265 (2008) 468–476.
[3] K.J. Kim, D.W. Moon, S.K. Lee, K.H. Jung, Formation of a highly oriented FeO thin film by phase transition of Fe_3O_4 and Fe nanocrystallines, Thin Solid Films 360 (2000) 118–121.
[4] N.K. Myshkin, H. Kong, A.Y. Grigoriev, E.S. Yoon, The use of color in wear debris analysis, Wear 251 (2001) 1218–1226.
[5] C. Rynio, H. Hattendorf, J. Klöwer, G. Eggeler, On the physical nature of tribolayers and wear debris after sliding wear in a superalloy/steel tribosystem at 25 and 300 °C, Wear 317 (2014) 26–38.
[6] S. Raadnui, Wear particle analysis utilization of quantitative computer image analysis: a review, Tribol. Int. 38 (2005) 871–878.
[7] H.K. Wu, T.H. Wu, Y.P. Peng, Z.X. Peng, Watershed-based morphological separation of wear debris chains for on-line ferrograph analysis, Tribol. Lett. 53 (2014) 411–420.
[8] T.H. Wu, J.Q. Wang, Y.P. Peng, Y.L. Zhang, Description of wear debris from on-line ferrograph images by their statistical color, Tribol. Trans. 55 (2012) 606–614.
[9] T.H. Wu, H.K. Wu, Y. Du, Z.X. Peng, Progress and trend of sensor technology for on-line oil monitoring, Sci. China Technol. Sci. 56 (2013) 2914–2926.
[10] E. Meijering, O. Dzyubachyk, I. Smal, Methods for cell and particle tracking, Methods Enzymol. 504 (2012) 183–200.
[11] C.C. Hua, Y.Q. Wang, X.P. Guan, Visual tracking control for an uncalibrated robot system with unknown camera parameters, Robot. Comput.-Integr. Manuf. 30 (2014) 19–24.
[12] Y.W. Wan, Y. Huang, B. Buckles, Camera calibration and vehicle tracking: highway traffic video analytics, Transp. Res. Part C 44 (2014) 202–213.
[13] O.P. Verma, P. Kumar, M. Hanmandlu, S. Chhabra, High dynamic range optimal fuzzy color image enhancement using Artificial Ant Colony System, Appl. Soft Comput. 12 (2012) 394–404.
[14] N.M. Kwok, H.Y. Shi, Q.P. Ha, G. Fang, S.Y. Chen, X. Jia, Simultaneous image color correction and enhancement using particle swarm optimization, Eng. Appl. Artif. Intell. 26 (2013) 2356–2371.
[15] J.K. Suhr, H.G. Jung, G. Li, J. Kim, Mixture of Gaussians-based background subtraction for Bayer-pattern image sequences, IEEE Trans. Circuits Syst. Video Technol. 21 (2011) 365–370.
[16] A. Sobral, A. Vacavant, A comprehensive review of background subtraction algorithms evaluated with synthetic and real videos, Comput. Vis. Image Underst. 122 (2014) 4–21.
[17] R Dash, B. Majhi, Motion blur parameters estimation for image restoration, Optik 125 (2014) 1634–1640.
[18] V.S. Hari, V.P.J. Raj, R Gopikakumari, Unsharp masking using quadratic filter for the enhancement of fingerprints in noisy background, Pattern Recognit. 46 (2013) 3198–3207.
[19] F. Lin, C. Jin, An improved Wiener deconvolution filter for high-resolution electron microscopy images, Micron 50 (2013) 1–6.
[20] A.M. Deshpandea, S. Patnaik, A novel modified cepstral based technique for blind estimation of motion blur, Optik 125 (2014) 606–615.
[21] D. Lee, J. Lee, Domain described support vector classifier for multi-classification problems, Pattern Recognit. 40 (2007) 41–51.
[22] Y. Zhang, Z.X. Chi, K.Q. Li, Fuzzy multi-class classifier based on support vector data description and improved PCM, Expert Syst. Appl. 36 (2009) 8714–8718.